X-RAY SPECTROMETRY
X-Ray Spectrom. **28**, 320–326 (1999)

Synchrotron Radiation X-Ray Fluorescence at the LNLS: Beamline Instrumentation and Experiments

Carlos A. Pérez,[1] Martin Radtke,[1] Héctor J. Sánchez,[2]* Helio Tolentino,[1] Regis T. Neuenshwander,[1] William Barg,[1] Marcelo Rubio,[3] María Izabel Silveira Bueno,[4] Ivo M. Raimundo[4] and Jarbas J. R. Rohwedder[4]

[1] Laboratorio Nacional de Luz Síncrotron–LNLS/CNPq, Caixa Postal 6192, 13038-970 Campinas, Brazil
[2] Facultad de Mátematica, Astronomía y Física, Universidad Nacional de Córdoba, 5000 Córdoba, Argentina
[3] CEPROCOR, Gobierno de Córdoba, Arenales 230, 5000 Córdoba, Argentina
[4] Instituto de Química, UNICAMP, Caixa Postal 6154, 13083-970, Campinas, Brazil

The x-ray fluorescence beamline of the Laboratorio Nacional de Luz Síncrotron (LNLS) is described. The main optical component of the beamline is a silicon (111) channel-cut monochromator, which can tune energies between 3 and 14 keV. A general description of two experimental stations is given. Beam characterization was done by measuring experimental parameters such as vertical profile and monochromatic flux. These results show that the photon flux at 8 keV in an area of 20 mm^2 is 4.2×10^9 photons s^{-1}. The possibility of achieving fine tuning of energies (high resolution) was confirmed. This paper presents some original results derived from the commissioning of the beamline, such as a comparison of detection limits in different experimental conditions, and a novel mechanical system to align capillaries together with a semi-automatic adjustment procedure. So far, there have been several proposals to perform a variety of experiments at this beamline, covering different fields, such as physics, chemistry, geology and biology.

INTRODUCTION

The Laboratorio Nacional de Luz Síncrotron (LNLS) is a national research center of the CNPq (National Council for Scientific and Technological Development), a division of the Brazilian Ministry of Science and Technology. It is located in Campinas, State of São Paulo, Brazil, and is the only synchrotron source in the southern hemisphere. The electron energy inside the storage ring is 1.37 GeV with a dipole magnetic field of 1.65 T. This gives a critical photon energy of 2.08 keV. The natural emittance is 100 nm rad and the revolution frequency is 3.2 MHz for this 93.2 m long machine.[1]

An x-ray fluorescence (XRF) beamline has been constructed at the LNLS. The synchrotron radiation source for the line is the DO9B (15°) bending magnet of the storage ring. The components of the line include one 125 μm beryllium window, to isolate the beamline vacuum from the ring vacuum and from atmosphere, a channel-cut crystal monochromator and a motorized computer-controlled set of slits to limit the beam size, before and after the monochromator. Figure 1 shows the beamline and its main components.

Both monochromatic and white beams can be used. For this reason, the monochromator vacuum chamber can be displaced allowing these two configurations. Since the intensity of the white beam is higher, aluminum filters must be used to avoid thermal damage of the beamline components.

Two experimental set-ups are mounted at the beamline. In the first, the total reflection x-ray fluorescence (TXRF) technique[2] can be used. Here, spectrochemical analysis with good detection limits of heavy and light elements is performed, and also surface analysis and depth-profiling studies by total reflection. In the second setup, μ-XRF analyses are performed, inspecting microscopic areas of the samples to give information about elemental distribution.[3]

Si(Li) and HPGe energy-dispersive detectors compose the detection system. Both detectors are placed at 90° to the incident beam. The whole set-up is mounted on a motorized lift table, which allows vertical positioning of instruments in the most polarized part of the beam. General-purpose detectors such as ionization chamber, photodiode and PIN diode are also available.

X-RAY OPTICAL ELEMENTS AT THE XRF BEAMLINE

Monochromator

The XRF beamline is equipped with a silicon (111) channel-cut crystal monochromator. It consists of a monolithic crystal with a slot in order to expose two parallel

* Correspondence to: H. J. Sánchez, Facultad de Mátematica, Astronomía y Física, Universidad Nacional de Córdoba, 5000 Córdoba, Argentina.
E-mail address: jsan@famaf.unc.edu.ar

CCC 0049–8246/99/050320–07 $17.50

Received 13 October 1998
Accepted 27 April 1999

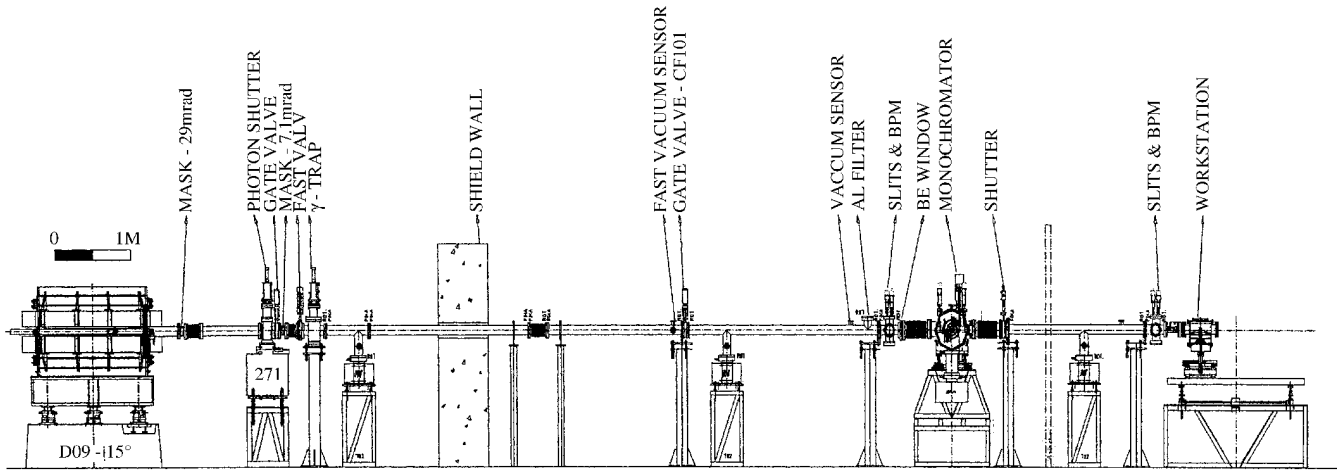

Figure 1. The XRF beamline and its components.

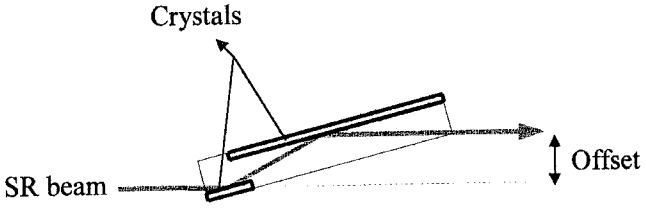

Figure 2. Outline of the channel-cut monochromator.

surfaces (Fig. 2). The white beam hits the first crystal face and reflects x-rays with wavelength λ, which satisfy the Bragg condition. This monochromatized beam hits the second crystal face, which reflects the beam along a parallel trajectory. Thus, as the crystal is rotated, the transmitted beam changes with a beam offset equal to $2l\cos(\theta)$, where l is the slot thickness and θ the Bragg angle. The crystal is located inside a high-vacuum chamber, which is maintained below 10^{-6} mbar using an ion pump. With this crystal, the energy can be tuned from 3 to 14 keV with a resolution of $(3-4) \times 10^{-4}$ between 7 and 10 keV.

Capillary optic

An x-ray microbeam a few micrometers in diameter is required for microanalytical techniques such as the synchrotron fluorescence microprobe. To be really useful for analytical applications, the microbeam should combine a large photon flux, small spot size and, in many cases, a wide energy range. This is a prerequisite to achieve high spatial resolution combined with low detection limits.

In recent years, capillary concentrators have turned out to be versatile optical elements for the production of synchrotron microbeams.[4] At the LNLS, two kind of capillaries are available at present: straight capillaries with a diameter between 10 and 100 μm and a length of 10 cm; and a conical-shaped capillary with an entrance diameter of 75 μm, an exit diameter of 13 μm and a length of 23.5 cm.

Kirkpatrick–Baez optic

Another microbeam optic, based on specular reflection on mirrors (focusing system), is under development. This optic consists of a pair of crossed meridional mirrors arranged in the so-called Kirkpatrick–Baez (KB) configuration[5] (Fig. 3). The system offers the possibility of having greater acceptance compared with capillary devices, so a large flux of photons could be collected. A large working distance could also be obtained. Limitations on the spatial resolution come mainly from the spherical aberration, so elliptical-shaped mirrors must be used. In our case, the mirrors would consist of optically flat surfaces that would be figured to a quasi-elliptical shape with the use of a mechanical bender.[6,7]

EXPERIMENTAL STATIONS

Total reflection x-ray fluorescence (TXRF) station

The TXRF station consists of a vacuum chamber ($\approx 5 \times 10^{-4}$ mbar working pressure) in which a goniometer is placed. Fine rotation can be achieved by the use of one high-resolution translation stage, coupled to a disc, by a thin steel wire. The translation stage of 0.5 μm per step with a disc of 59 mm radius produces a 10 μrad angular

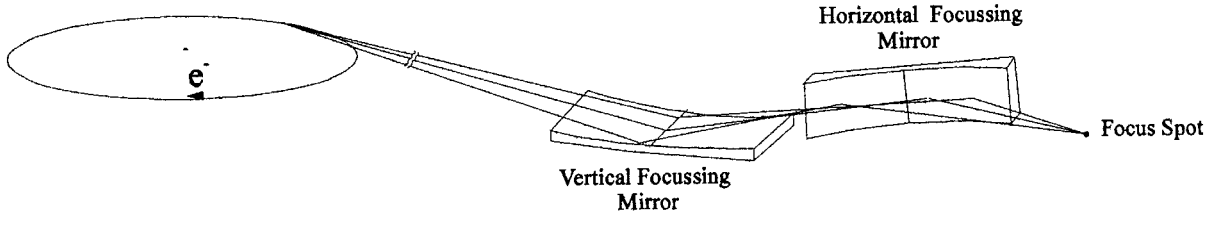

Figure 3. The Kirkpatrick–Baez configuration.

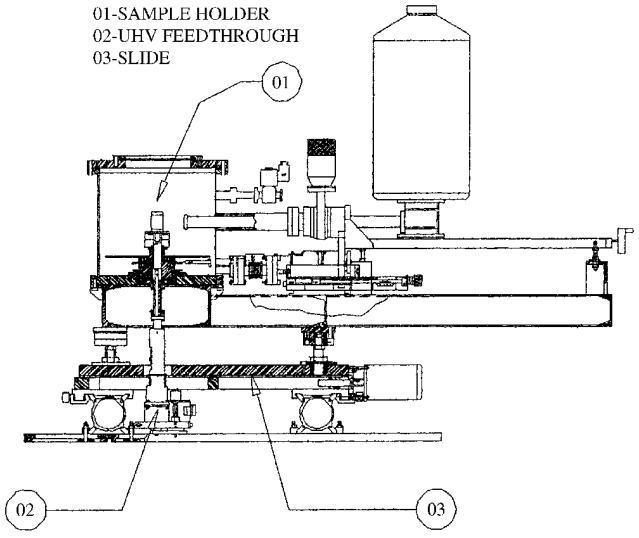

Figure 4. Drawing of the TXRF station.

resolution. The angular range extends from 0 to 19°. The positioning of the sample on the beam path can be done by using a UHV linear feedthrough, placed at the bottom of the chamber and coupled to the sample holder, and moving the whole experimental station on a slide. In both cases, the precision on the movements is around 2 μm. All the motions needed to adjust total reflection on translation and rotation stages are fully remote controlled. A drawing of the TXRF station is shown in Fig. 4.

Micro-x-ray fluorescence (μ-XRF) station

This set-up consists of a capillary alignment table that was designed for repeatability and high angular resolution as well as complete translational capacity. Four linear translation stages were mechanically coupled with flexible linkages to provide translations and rotations perpendicular to the capillary longitudinal axis. Movements of the linear translation stages of the same sign result in horizontal or vertical motions. Movements of opposite signs result in angular displacements of the capillary. Figure 5 shows the drawing of this set-up.

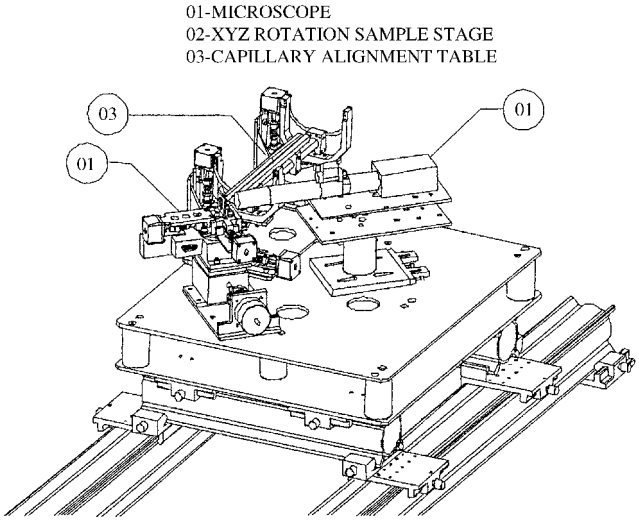

Figure 5. Drawing of the microfluorescence station.

The use of a capillary requires careful alignment of the four degrees of freedom that the capillary alignment table provides. To support the user in the complicated task of aligning, a new unit was created in the standard beamline software package. This unit takes care of two time-consuming actions. First, it aligns the capillary support parallel to the incoming beam. Once the support is aligned, the horizontal position can be fixed and the problem is reduced from four to two degrees of freedom. Then, it is relatively easy to get a small fraction of the beam through the capillary. If a sufficient amount of intensity is detected, the fine adjustment can be done automatically. The Powell algorithm[8] controls the optimization. The signal, which has to be optimized, is the current of an ionization chamber behind the capillary. The four motor positions of the alignment table serve as free parameters.

The μ-XRF station also includes an optical microscope with motorized zoom, and X, Y, Z, θ_z sample stages that are fully remote controlled.

BEAM CHARACTERIZATION

Vertical profile

The vertical profile of the monochromatic and white beam was measured. In both cases, the intensity of the x-ray beam was collected using a photodiode (IRD, Model AXUV-20HE1) with 100% efficiency between 100 eV and 12 keV, and a slit of 50 μm vertical size. The vertical scan was made in 50 μm steps, from the lower to the upper part of the beam. For the vertical profile of the white beam, a thick aluminum filter was used to attenuate the high flux of photons and thus to avoid damage in the detection system. Figures 6 and 7 show the profiles for a 7 keV monochromatic beam and for the white beam, respectively.

Beam intensity

The monochromatic flux of photons for four energies was measured. In this case, the entrance slits of the monochromator were set to 5 and 4 mm for the vertical and horizontal directions, respectively. The flux of photons was

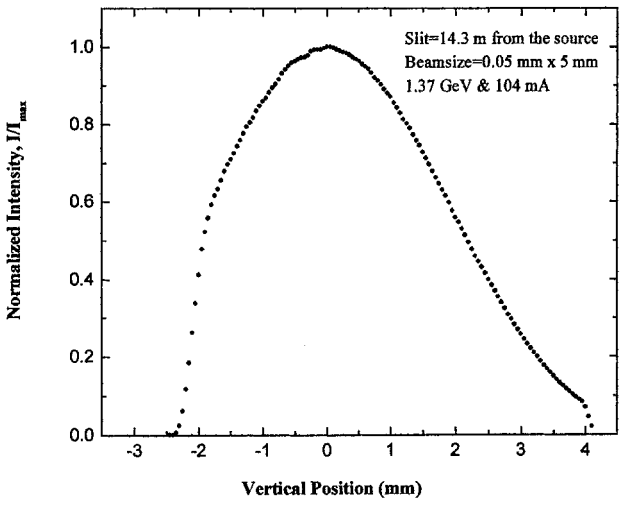

Figure 6. Vertical profile of a 7 keV monochromatic beam.

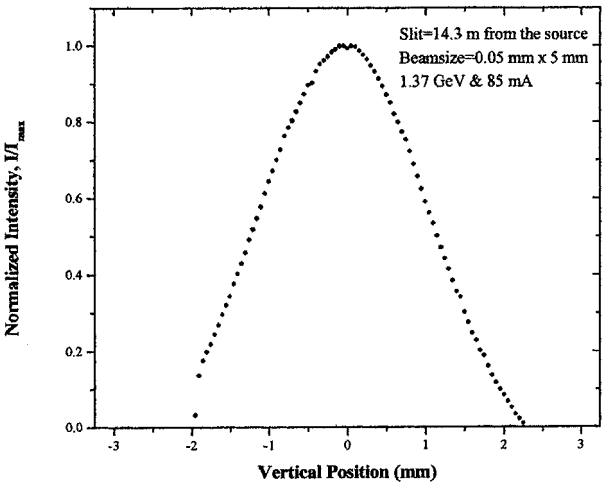

Figure 7. Vertical profile of the white beam.

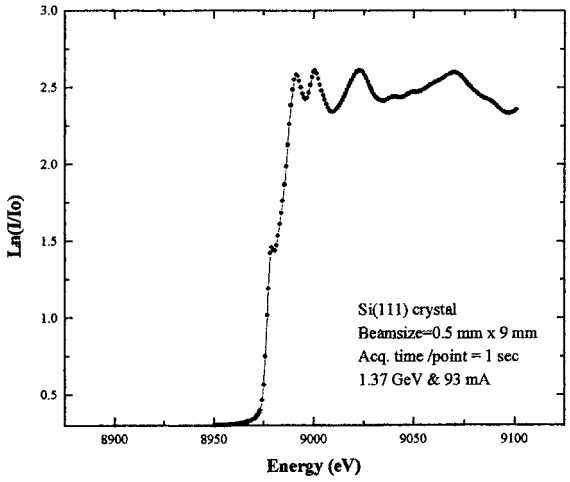

Figure 8. The absorption Kα edge of Cu measured with the channel-cut monochromator.

Table 1. Monochromatic flux measured and calculated at different energies

Energy (keV)	Current (mA)	Measured flux (photons s^{-1})	Calculated flux (photons s^{-1})
7	104	$5.0\ 10^9$	$9.1\ 10^9$
8	102	$4.2\ 10^9$	$6.0\ 10^9$
9	100	$3.0\ 10^9$	$3.9\ 10^9$
10	100	$2.0\ 10^9$	$2.6\ 10^9$

measured on the whole active area of the photodiode (20 mm^2), placed at 14.3 m from the source. The measured values are shown in Table 1, compared with the theoretical values, calculated using a utility program from SHADOW code.[9]

Energy resolution

In order to investigate the energy resolution of the monochromator, an EXAFS experiment in the transmission mode[10] was performed. For this purpose, the near-absorption K-edge of Cu was scanned by fine tuning of the incident energy. This proved the ability of the monochromator to tune energies with high resolution. Two ionization chambers, before and after the sample, performed the experiment. The sample consisted of a Cu foil of 12.5 μm thickness. During the experiment, the energy was changed in steps of 1 eV and the data from the ionization chambers were collected. Figure 8 shows the results for the EXAFS spectrum.

Microbeam profile

Several straight capillaries and one of conical shape were tested. For all capillaries the beamsize was determined by a knife-edge scan, using a thin gold foil. An example of the measured intensity distribution is given in Fig. 9.

For the conical capillary the beamsize was also measured as a function of the distance from its tip to the sample position. The results are shown in Fig. 10. Because of the geometry used, a distance of less than 1 mm was reached.

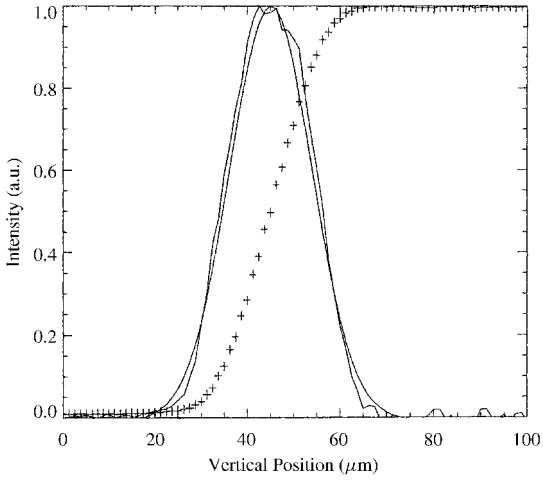

Figure 9. Knife edge scan of the conical capillary for 0.8 mm distance between sample and capillary exit. The figure shows an FWHM of 20 μm. +, Measured data; ---, first derivative; ——, Gaussian fit.

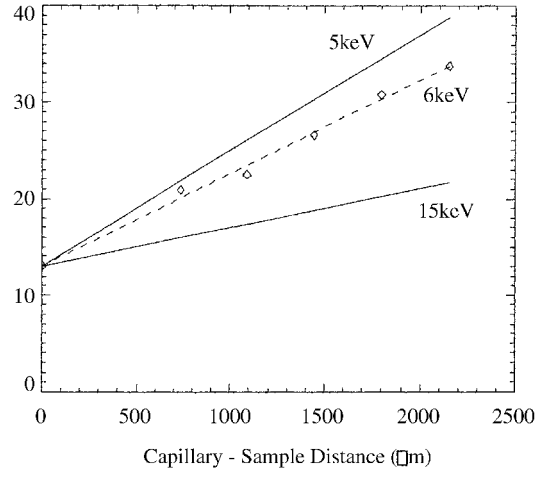

Figure 10. Measured beamsize as function of the sample to capillary distance. The measured points show a good correlation with the theoretical values calculated for 6 keV.

The gain factor of the conical capillary was calculated for the white beam. The gain factor is defined as the ratio

Table 2. Measured parameters used to calculate the gain factor

Capillary	Straight	Conical
Beam diameter (μm)	50	13
Area (μm^2)	1963	133
Intensity (a.u.)	269192	317037
Current (mA)	84.8	81.8
Intensity/(area × current)	1.61	29.14
Gain	—	18

of the number of photons to the area of the focused and unfocused beam. The intensity of the unfocused beam was measured with a straight capillary of 50 μm diameter. The minimum beamsize at the exit diameter of the capillary was used. Table 2 shows the value for the gain factor together with different measured parameters.

MINIMUM DETECTION LIMIT SURVEYS

Several measurements of standard samples in total reflection conditions were carried out in order to determine minimum detection limits (MDL).[11] The standard samples (see Table 3) were prepared by evaporating 10 μl of different solutions on quartz substrates. The solutions were composed of 10 ml of triply distilled water, 0.1 ml of gallium solution (internal standard) and different quantities of a standard solution (Aldrich Chemical, no 41399-2, in 5% HNO_3). All samples were excited in air using the full synchrotron radiation spectrum. Sample B was chosen to irradiate with monochromatic beam at 9 keV, in a low-vacuum environment. Figures 11 and 12 show the MDL as a function of the atomic number *Z*. The values were extrapolated to a measuring time of 1000 s according to generally accepted conventions.[12] From Fig. 11 we can observe increasing values of the MDL with increase in concentration, as a consequence of the higher contribution to the background from the sample itself. Figure 12 shows the values of the MDL for sample B, measured under three different experimental conditions. In the case of monochromatic excitation, slight improvements in the MDL can be observed when a low-vacuum environment is used. On the other hand, we did not obtain better improvements of the MDL using monoenergetic excitation compared with the full spectrum excitation.

Table 3. Values of the concentration of the selected elements in different standard samples

Element	A (ppm)	B (ppm)	C (ppm)	D (ppm)
V	0.971	1.905	3.67	4.504
Cr	0.388	0.762	1.468	1.802
Mn	0.971	1.905	3.67	4.504
Fe	1.942	3.809	7.34	9.009
Co	0.971	1.905	3.67	4.504
Ni	0.971	1.905	3.67	4.504
Cu	0.485	0.952	1.835	2.252
Zn	0.971	1.905	3.67	4.504
Ga	9.951	9.762	9.404	9.234
As	3.883	7.619	14.679	18.018
Se	3.883	7.619	14.679	18.018

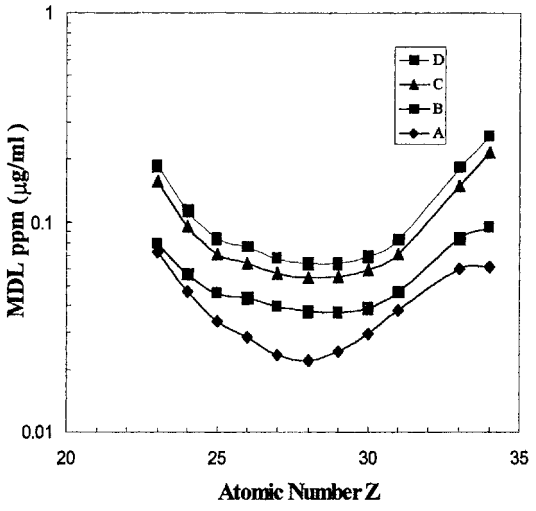

Figure 11. MDL as a function of the atomic number *Z* for different samples.

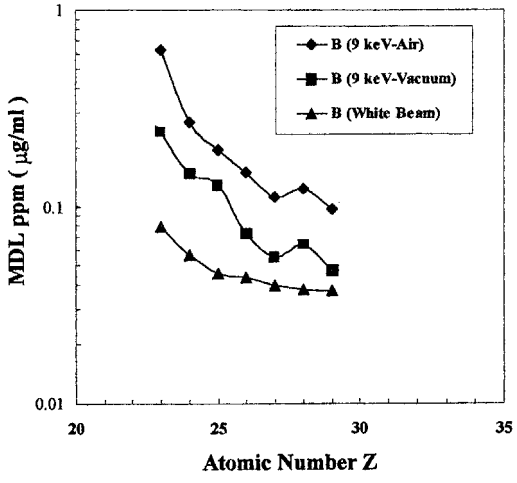

Figure 12. MDL as a function of the atomic number *Z* for sample B.

In general, the values of MDL obtained are in good agreement with those reported by other workers in different synchrotron radiation facilities.[13]

The station allows for conventional XRF analysis and total reflection XRF analysis in grazing incidence (GIXRF)[14] or grazing exit (GEXRF)[15] conditions. The most important result, regarding the different experimental configurations, is a survey of detection limits for the elements of the same specimen in the three cases, with monochromatic or white excitation. The sample consists of a few milligrams of a fine powder of hydroxyapatite with 200 ppm Zn, deposited on a silicon wafer, covering an area of 25 mm^2. The whole sample was irradiated consecutively using the three experimental conditions (conventional XRF, GIXRF and GEXRF) with a white beam and monochromatic beam of 5 and 9.7 keV, respectively. The results are summarized in Table 4. It should be remarked that the aim of this experiment was not to obtain the optimum detection limit but to compare different techniques with exactly the same sample. As can be seen in Table 4, any total reflection technique produces detection limits one order of magnitude or more better than conventional XRF with a monochromatic beam. Although, in general, monochromatic photons improve the detection

Table 4. Detection limits for an apatite sample (with 200 ppm of Zn) using different XRF techniques

Technique	P (ppm)	Ca (ppm)	Zn (ppm)
Conventional (5 keV)	2310	155	—
Conventional (9.7 keV)	3330	211	15
GEXRF (white beam)	800	27	13
GIXRF (5 keV)	200	16	—
GIXRF (9.7 keV)	280	20	0.2
GIXRF (white beam)	33	0.8	1

limits, the best results are obtained in GIXRF with the white beam. This can be explained by considering that the critical energy of the storage ring is 2.08 keV, then the white spectrum has very high intensity for low energies (in the total reflection regime) and low intensity for high energies (outside the total reflection regime). In this situation, an extremely high incident intensity is mandatory for the reduction of detection limits.

FUTURE APPLICATIONS

The XRF beamline was designed so as to take advantage of the synchrotron radiation characteristics. In principle, the synchrotron radiation x-ray fluorescence (SR-XRF) technique is especially efficient for spectrochemical analysis when the amount of sample is very small.

In the case of TXRF analysis, multielement analysis in the sub-nanogram range becomes possible. This is important in forensic, environmental and biological studies. The use of the grazing incidence XRF and grazing exit XRF allows one to perform surface analysis in multilayers, wafers and implanted semiconductors. The x-ray fluorescence microprobe (μ-XRF) technique opens up multiple application fields, and gives the possibility of determining the dependence of concentrations on the position of multielement samples. Usually, this kind of experiment cannot be achieved with the classical microprobe techniques. The fields of application extend to all kind of experimental science, including medicine, forensic and technology (materials and microstructures), and also applied research in archaeology, art and cultural history. In these fields the detection of position-dependent traces helps to determine the age and cultural or personal classification of the investigated specimens.

The SR-XRF microprobe is also important in geoscience. There, it allows the characterization of minerals, phase boundaries and inclusions by analysis of trace elements.

CONCLUSIONS

The XRF beamline is now in operation at the LNLS. The feasibility of selecting elements by fine tuning the energy has been shown. It was found that, for good energy resolution, a highly collimated incident beam must be used. In this way, the energy resolution is limited only by the natural Darwin width of the crystal.[16] It is important to point out that in most x-ray fluorescence applications which involve the use of monochromatic excitation, high energy resolution is not always necessary, so a larger beamsize is often used to increase the photon flux impinging on the sample. In the future, the use of a silicon crystal with (200) orientation will allow the selection of energies between 15 and 23 keV. The use of a mosaic crystal instead of a perfect crystal sacrifices energy resolution but delivers a higher flux of photons, as an alternative.

To develop experiments related to TXRF, a high-vacuum chamber was assembled. The set-up includes fine rotation and vertical translation stages for positioning the sample, and an energy-dispersive solid-state detector equipped with an HPGe crystal. The combination of energy resolution and the possibility of using an ultra-thin window will allow in the future greater efficiency in the detection of light elements.

In this paper we have described a novel mechanical system for capillary alignment installed at the μ-XRF station. The set-up includes a computer program able to carry out the semi-automatic control of the fine adjustment movements. The main part of this program uses the Powell algorithm that maximizes the count rate of an ionization chamber as a function of the motor positions. A fully automatic alignment procedure is still under development.

The measured microbeam profile shows that a 20 μm beamsize diameter can be obtained at 0.8 mm from the tip of the conical capillary. From our measurements we have also seen that a gain factor of 18 for the white beam is obtained on the sample, provided that it remains as near as possible to the capillary exit diameter.

The survey of detection limits, for the same sample under different experimental conditions (carried out during the commissioning), shows the advantages of total reflection techniques and the importance of achieving the maximum photon flux on the sample.

As a final comment, it should be mentioned that, after the commissioning, the XRF beamline is available for use by the national and international community.

REFERENCES

1. A. R. D. Rodrigues, R. H. A. Farias, M. J. Ferreira, G. S. Franco, L. C. Janhnel, L. Lin, A. C. Lira, R. T. Neuneschwander, C. Pardine, F. Rafael, A. Rosa, C. Scorzato, C. E. T. Gonçalves da Silva, A. Romeu da Silva, P. F. Tavares, D. Wisnivesky and A. Craievich, presented at the Particle Accelarator Conference, PAC97, Vancouver, 1997.
2. C. Streli, P. Wobrauscheck, W. Ladisich, R. Rieder, H. Aiginger, R. W. Ryon and P. Pianetta, *Nucl. Instrum. Methods* **345A**, 399 (1994).
3. K. Janssens, L. Vincze, B. Vekemans, A. Aerts, F. Adams, K. W. Jones and A. Knochel, *Mikrochimi. Acta* **13** (Suppl.), 87 (1996).
4. D. J. Thiel, D. H. Bilderback and A. Lewis, *Proc. SPIE* **1740**, 248 (1992).
5. P. Kirkpatrick and A. V. Baez, *J. Opt. Soc.* **38**, 766 (1948).
6. H. A. Padmore, M. R. Howells, S. Irick, R. Sandler and Y.-M. Koo, *Proc. SPIE* **2856**, 145 (1996).
7. P. J. Eng, M. Rivers, B. X. Yang and W. Schildkamp, *Proc. SPIE* **2516**, 41 (1995).
8. W. H. Press, B. P. Flannery, S. A. Teukolsky and W. T. Vetterling, *Numerical Recipes: the Art of Scientific Computing.* Cambridge University Press, Cambridge (1988).
9. C. Welnak, P. Anderson, M. Khan, S. Singh and F. Cerrina, *Rev. Sci. Instrum.* **63**, 865 (1992).

10. E. Stern and S. M. Heald, in *Handbook on Synchrotron Radiation*, Vol. 1, Edited by E. Koch, pp. 955–1014. North-Holland, New York (1983).
11. P. Kump, *Spectrochim. Acta, Part B* **52**, 405 (1997).
12. W. Ladisich, R. Rieder, P. Wobrauscheck and H. Aiginger, *Nucl. Instrum. Methods* **330A**, 501 (1993).
13. A. J. J. Bos, R. D. Vis, H. Verheul, M. Prins, S. T. Davies, D. K. Bowen, J. Makjanic and V. Valcovic, *Nucl. Instrum. Methods* **B3**, 232 (1984).
14. W. Yun and J. M. Bloch, *J. Appl. Phys.* **68**, 1421 (1990).
15. P. K. De Bokx and H. P. Urbach, *Rev. Sci. Instrum.* **66**, 15 (1994).
16. B. W. Batterman and D. Bilderback, in *Handbook on Synchrotron Radiation*, Vol. 3, Edited by G. Brown and D. E. Moncton, pp. 105–153. North-Holland, New York (1991).